BEAM PERFORMANCE OF THE 10-MEV SECTION OF THE 200-MEV LINEAR ACCELERATOR AT BROOKHAVEN NATIONAL LABORATORY*

K. Batchelor, J. Bittner, R. Chasman,
N. Fewell, T. Sluyters, and R. Witkover
Brookhaven National Laboratory
Upton, New York 11973

ABSTRACT

Performance of the new 10-MeV linac and its low energy transport system will be illustrated by means of partial emittances, intensities, density distributions and energy and phase spreads. Special emphasis will be put on the influence of space charge on the transverse and longitudinal properties of the beam. Comparison will be made between experimental data and computational results.

Introduction

Early in the design stages of the new 200-MeV proton linear accelerator injector for the BNL Alternating Gradient Synchrotron it was decided that in order to establish correct operating levels for the preinjector, the low energy beam transport system (LEBT) and tank No. 1, a series of calibration measurements should be performed before the installation of tank No. 2. This report gives details of the computations and measurements made both prior to and during this calibration period.

Equipment

Complete details of the equipment used for the 200-MeV linac will be given in other papers to be presented at this conference so only a brief summary will be given here. Figure 1 is a schematic diagram of the equipment involved. The ion source is of the duoplasmatron type[1] with a large expansion cup and delivers up to 400 mA peak proton current. The high gradient column[2] operates up to a voltage of 830 kV and at the output end houses a 4-in. diameter aperture pulsed quadrupole triplet which is the first focusing element of the LEBT system used to transport the beam from the preinjector to tank No. 1. This LEBT system has seven more quadrupole triplets at approximately 1-m spacing. There are five viewing boxes capable of containing both horizontal and vertical emittance devices simultaneously and a beam transformer for beam current measurement. LEBT also contains the two 200 MHz bunchers which are capable of operation up to voltages in excess of 35 kV. Detailed design of the LEBT system is described in reference 3. Complete details of the cavity, rf system, quadrupole and

*Work performed under the auspices of the U. S. Atomic Energy Commission.

vacuum system designs are presented in other papers at this conference.[4-7] Figure 1 also shows the equipment arrangement at the output end of tank No. 1. The first viewing box VB6 contains an adjustable slit, a beam transformer and either a quartz plate for viewing the beam spot size with a TV camera or an automatic electronic emittance device[8] for radial emittance measurements. The second viewing box VB7 contains a rotatable energy degrading foil, two beam transformers and a faraday cup. The quadrupole triplet in this line is designed to produce an image of the adjustable slit in VB6, at the slit and collector in the end of the beam line beyond the bending magnet for use in momentum analysis.

Diagnostic Techniques

The method used to measure the transverse emittance of the beam is described by N. Fewell and R. Witkover in a paper to be presented at this conference.[8] Figure 2 shows the method used to measure momentum. The bending magnet power supply reference voltage was remotely adjusted to sweep the magnet current and hence moved the beam across the 0.020-in. wide slit in front of the current collector, the signal from which was amplified and fed to the Y plates of a storage oscilloscope in the control room. A precision shunt in the magnet power supply provided, with suitable dc biasing and amplification, the signal to the X plates of this oscilloscope. Either the ion source trigger pulse or a beam current pulse from a beam transformer was used to trigger a pulse generator with adjustable gain, pulse delay and pulse width which provided the Z axis modulation for the oscilloscope. Thus the sample width and time during the beam pulse could be selected. Tank rf levels were measured in a slide-back arrangement using a Hewlett-Packard type HP5082-2800 hot carrier diode with up to 30 V of dc bias. The rf level values quoted in this report are helipot settings for the bias voltage and are directly proportional to cavity field. The field was measured with the cavity in the beam loaded condition. Phase shifts between each buncher and the tank were measured using a Hewlett-Packard 10514A double-balanced mixer. A signal from a buncher and the tank were each fed into one arm of the mixer. As the tank phase was changed, the mixer balance was restored by adjusting a calibrated phase shifter connected in series with the tank input arm of the mixer. The signal level without beam loading was used as a null indicator so that there was correspondence of actual phase shifter readings at different beam current levels. Typical phase and amplitude signals are given in reference 9.

Computational Methods

Two basic computer programs were used to provide the theoretical data for comparison with the measurements. The LONMO program described by A. Benton[10] was used for data taken at low beam currents and without bunchers, whereas the six-dimensional program with space charge described by R. Chasman in reference 11 was used for comparison at high current levels.

Beam Measurements

Adjustment of the Preinjection Energy and Tank No. 1 RF Level

Plots of Tank No. 1 transparency (i.e., ratio of output to input beam currents) were made for a number of rf field levels in tank No. 1. These plots were compared with data computed using the LONMO program and this comparison between the two sets of data allowed an estimate of the correct preinjector voltage setting and tank No. 1 rf level setting to be made (see Fig. 3).

Further checks of the tank rf level were made by comparing computed spectra with measured spectra at three different injection energies of 730, 750 and 770 keV (Figs. 4, 5 and 6). It can be seen that these three sets of data are consistent with a tank rf level setting of ~ 545 for the design value. Furthermore, the general change of shape of the measured spectra with increasing rf field levels can be seen to be following the pattern of the computed spectra. The definition of the measured data was estimated to be ~ 70 keV, whereas the definition of the computed data was ~ 40 keV. This difference in definition gives a broadening of the measured spectra (and a smoothing of the peaks) compared with the computed spectra. Typical shifts in mean 10-MeV energy due to the 20-keV difference in injection energy were ~ 40 keV, the direction depending on the number of phase oscillations executed by the protons at that particular rf level. Collimators in the LEBT system were used to produce a low current parallel beam for this set of measurements.

Optimization of Bunchers

Having established preinjector and tank No. 1 operating levels, buncher No. 2 was turned on and phased with respect to tank No. 1 by observing 10-MeV current as a function of buncher/tank phase for the design rf level and a Cockcroft-Walton voltage of 770 kV. These data, plotted in Fig. 7, gave an optimized operating level of 24 kV for buncher No. 2 with a buncher/tank phase setting of 100 degrees on the arbitrary scale used. Buncher No. 2 was set at the above voltage and average 10-MeV momentum measured as a function of buncher/tank phase for a number of rf levels. The resulting data are compared in Fig. 8 with data computed using the LONMO program without space charge. It can be seen that there is reasonably good agreement between this oversimplified theory and practice and that the rf level reading of 545 is the indicated design value. The plots do not pass through a single point due to the method used to measure the buncher/tank phase which does not take account of the phase shift due to beam loading. Buncher No. 1 was then turned on and an operational voltage level determined by running a series of buncher No. 1/buncher No. 2 phase runs for different buncher No. 1 and buncher No. 2 voltage levels and optimizing for maximum beam current. The detailed data for each run were not plotted but settings of both buncher voltages were determined as 18.5 kV for buncher No. 1 and 25 kV for buncher No. 2. A beam current plot as a function of bunchers/tank phase for three tank rf levels is also plotted in Fig. 9 where the maximum recorded beam current was 210 mA. In Fig. 10 the spectra correspond-

ing to this data are shown together with a theoretical mean energy shift plot calculated using the LONMO program. Table I lists all machine operating conditions for the 210-mA beam. To complete the energy data, spectra were taken at different times during a 140 μsec beam pulse in order to look at the during-the-pulse stability of the beam. Both rf phase and amplitude control loops were closed when these data were taken. The results as seen in Fig. 11 show little change of spectra during the pulse.

TABLE I

Operating Valves for 210 mA, 10 MeV Beam Current Preinjector and Ion Source

Cockcroft-Walton Voltage = 780 kV.

Bouncer High Voltage = 30 kV, Current = 4.4 mA.

780 keV Beam Current (BT1) = 400 mA, Beam Pulse Length - 30 μsec.

Low Energy Beam Transport System

Triplet No. 1; - Quadrupoles Q1 and Q3 = 239A, Quadrupole Q2 = 193A.
Triplet No. 2; - Quadrupoles Q4 and Q6 = 100A, Quadrupole Q5 = 133A.
Triplet No. 3; - Quadrupoles Q7 and Q9 = 187A, Quadrupole Q8 = 183A.
Triplet No. 4; - Quadrupoles Q10 and Q12 = 101A, Quadrupole Q11 = 176A.
Triplet No. 5; - Quadrupoles Q13 and Q15 = 157A, Quadrupole Q14 = 134A.
Triplet No. 6; - Quadrupoles Q16 and Q18 = 108A, Quadrupole Q17 = 154A.
Triplet No. 7; - Quadrupoles Q19 and Q21 = 177A, Quadrupole Q20 = 174A.
Triplet No. 8; - Quadrupoles Q22 and Q24 = 214A, Quadrupole Q23 = 224A.
Buncher No. 1 Voltage = 18.5 kV, Buncher No. 2 Voltage = 25 kV, Bunchers in Phase.
BT1 = 400 mA; BT2 = 400 mA; BT3 = 430 mA; BT4 = 400 mA; BT5 = 275 mA; BT6 = 280 mA.

Tank No. 1

RF Reference Potentiometer = 560 = 1.025 X Design Value.

Quadrupoles Q1 - 1 = 93A; Q1 - 2 = 174A; Q1 - 3 and Q1 - 4 = 201A:
Q1 - 5 and Q 1 - 6 = 201A; Q1 - 7 and Q1 - 8 = 201A; Q1 - 9 and Q1 - 10 = 147A;
Q1 - 11 and Q1 - 12 = 156A; Q1 - 13 and Q1 - 14 = 156A; Q1 - 14 and Q1 - 16 = 134A;
Q1 - 17 and Q1 - 18 = 162A; Q1 - 19 and Q1 - 20 = 212A; Q1 - 21 and Q1 - 22 = 199A;
Q1 - 23 and Q1 - 24 = 202A; Q1 - 25 and Q1 - 26 = 207A; Q1 - 27 and Q1 - 28 = 197A;
Q1 - 29 and Q1 - 30 = 199A; Q1 - 31 and Q1 - 32 = 193A; Q1 - 33 and Q1 - 34 = 201A;
Q1 - 35 and Q1 - 36 = 208A; Q1 - 37 and Q1 - 38 = 120A; Q1 - 39 and Q1 - 40 = 125A;
Q1 - 41 and Q1 - 42 = 109A; Q1 - 43 and Q1 - 44 = 106A; Q1 - 45 and Q1 - 46 = 127A;
Q1 - 47 and Q1 - 48 = 141A; Q1 - 49 and Q1 - 50 = 161A; Q1 - 51 and Q1 - 52 = 149A;
Q1 - 53 and Q1 - 54 = 163A; Q1 - 55 and Q1 - 56 = 81A; Q1 - 57 off Q2 - 1 = 146A.

Field Gradient Values for Quadrupoles

Triplet No. 1; 1.74 G/cm/A for lengths 14.4 cm outer and 23.4 cm inner.
Triplets No. 2 - 7; 3.10 G/cm/A for lengths 12.1 cm outer and 20.8 cm inner.
Triplet No. 8; 6.67 G/cm/A for lengths 6.4 cm outer and 10.1 cm inner.
Q1 - 1 = 4.01 kG/cm; Q1 - 2 = 7.24 kG/cm; Q1 - 3 to Q 1 - 8 = 6 $\approx$ 21 kG/cm;
Q1 - 9 and Q1 - 10 = 6.21 kG/cm; Q1 - 11 to Q1 - 14 = 6.55 kG/cm;
Q1 - 15 and Q1 - 16 = 5.97 kG/cm; Q1-17 and Q1 - 18 = 6.78 kG/cm;
Q1 - 19 to Q2 - 1 = 22.7 G/cm/A.

Quadrupole Lengths

Q1 - 1 to Q1 - 8 = 2.54 cm; Q1 - 9 to Q1 - 18 = 3.17 cm;
Q1 - 19 to Q1 - 36 and Q1 - 57 and Q2 - 1 = 4.44 cm; Q1 - 37 to Q1 - 56 = 6.98 cm.

Transverse Beam Properties

Emittance measurements were performed in LEBT at the output of the preinjector (VB1), in front of the linac (VB5), and after the 10-MeV cavity (VB6).

Emittance Measurements in LEBT. Figure 12 shows a typical emittance observed in VB1 at the output of the preinjector from a beam whose source characteristics are summarized in Table II. The horizontal and vertical resolutions in this picture are 0.5 mm and 2 mrad respectively. As can be easily ascertained, two different beams are visible. Both of these beams consist of H^+ ions since the H_2^+ molecular content from the source is discriminated against by the threshold level of the emittance device. The intensity of the broad and divergent proton beam is very low as can also be seen from the results of the beam profile measurements, which are shown in the lower part of Fig. 12. The appearance of the two proton beams can be explained assuming a particular shape of the plasma boundary in the large expansion cap.

Figures 14 and 15 show results of measurements in VB5 situated close to the linac entrance. At this point, the molecular component of the beam has already been dispersed in the long transport channel preceding it. The proton beam here is converging into the small aperture of the linac. The quadrupoles of the first and second drift tubes are operated below the values corresponding to the "gradient law" of the linac so that a proper match can be made at the third drift tube to the periodic + - + - focusing structure. This avoids excessive gradients in the triplet between buncher No. 2 and the tank.

Typical emittances in two phase planes, each representing more than 80% of the proton beam, are shown in Fig. 15. The horizontal and vertical resolutions in these pictures are 0.5 mm and 2.5 mrad respectively.

Though only few emittance measurements were made directly after the preinjector, i.e., in VB1, there is an indication that the emittance at this point is about 30% smaller than those measured at the entrance of the linac. This growth in phase space

area seems to be independent of whether the bunchers were energized or not.

Emittances for different proton currents are shown in Fig. 14. These were obtained from measurements in which the LEBT quadrupoles were adjusted for maximum transmission through the transport system.

Emittance Measurements After 10-MeV Linac Section. The 10-MeV emittance measurements were performed in VB6 at a distance of 1.75 m away from the linac tank. The gradients in the last three quadrupoles of the tank were lowered from the design values in order to minimize beam losses in the drift section between the linac and VB6.

A typical emittance pattern of the beam in VB6 is shown together with its profile in Fig. 16. The horizontal and vertical resolutions are 0.5 mm and 2 mrad respectively.

Values of 10-MeV emittances for different proton currents are shown in Fig. 17.

Figure 18 shows phase space areas in the y-y′ plane for different percentages of the beam before as well as after the 10-MeV linac section. These emittances were recorded during a run in which a single buncher (No. 2) was used, resulting in 55% tank transmission. Input and output currents were 220 mA and 120 mA respectively. Also shown for comparison are results of measurements with neither buncher energized. The somewhat smaller emittances that were observed with the bunchers de-energized could easily be explained by a reduction of space charge effects in the beginning of the linac under these conditions.

Transverse beam properties of a 200-mA linac output beam are shown in Fig. 19 together with the corresponding input conditions. This beam current was achieved with both bunchers in operation, resulting in a 72% linac capture efficiency. The phase space areas at the linac entrance are identical in both planes. However, at the output the emittance area in the x-x′ plane is considerably smaller than that in the y-y′ plane. The ratios or normalized output to input emittances for different percentages of the beam are shown in Fig. 20.

Emittance areas before and after the 10-MeV tank are shown in Fig. 13 as a function of time during the 140 μsec beam pulse. The phase space area seems to be independent of time except during the first 20 μsec which is the rise time of the beam pulse.

Numerical Calculations. Data from measurements with the 200-mA linac output current were used for computer calculations in order to enable comparison of measured and calculated transverse beam properties at high current levels.

The input distributions in transverse phase space, used in the calculations, were similar to the emittances which were measured in VB5. Beam displacements in the x′ and y′ coordinates which had been observed during the emittance measurements were neglected because these initial offsets in two phase planes might have been required to compensate for unknown linac misalignments in order to get maximum current transmission. Since no corresponding emittances were measured in front of the bunchers, the

input distribution in longitudinal phase space had to be obtained from a computer run which simulated the beam through the two bunchers (using measured buncher parameters) up to the linac entrance. The transverse beam properties that were used in this run were not derived from any measurements, but were taken from other computer runs that had been made earlier for the design of the transport system.

The beam was simulated through the linac up to VB6 using measured values for the input current, injection energy, rf level and linac quadrupole settings. A capture efficiency of 68% was obtained compared to the value of 72% which was observed experimentally. Figure 21 shows the phase space projections of the computer-simulated beam at the center of drift tube 3 where the beam should have been matched to the acceptance of the linac. The superimposed ellipses, also shown in this figure, are the contours in two phase planes of a properly matched beam taking into account measured values of emittances, current, rf level and quadrupole gradients in the tank. One can easily see from Fig. 21 that proper matching conditions were not achieved by simply adjusting the quadrupoles in LEBT and the first two drift tubes of the tank for maximum current transmission through the linac.

Figure 22 shows the phase space projections of the simulated beam at VB6 together with the contours of the emittances which were measured at this point for 92% of the beam. Reasonable agreement was obtained between measured and computed emittances as can be easily ascertained from the figure.

Ratios of normalized output to input rms emittances were also obtained from the computations. These were roughly equal in the two phase planes and showed phase space dilution by factors of 2 to 3 for different percentages of the beam, which is not inconsistent with the experimentally obtained values for emittance growth (see Fig. 20).

It should be pointed out, that for the same basic beam and machine parameters, earlier numerical calculations of space charge effects in bright linac beams [12,13] predicted a much smaller emittance growth than was both measured and calculated in this work. The cause for the apparent discrepancy may very well be the absence of proper matching conditions at the entrance of the linac as was demonstrated in Fig. 21. Results of earlier computations[12] emphasized the importance of well-matched beams for minimum emittance growth. One can therefore hope that by an improved matching procedure, better beam quality will eventually be achieved. More complete measurements and calculations are needed for better quantitative understanding.

Acknowledgments

The authors wish to acknowledge the work of all members of the Linac Staff, without whose dedication and effort the results presented here would not have been possible. The theoretical and computational work of C. Agritellis, A. Benton, R. L. Gluckstern, and of the Physical Sciences Laboratory of the University of Wisconsin is gratefully acknowledged. The many helpful discussions with members of the National Accelerator Laboratory and the Los Alamos Scientific Laboratory were also much appreciated.

References

1. Th. J. M. Sluyters, "Some Considerations Associated with High Current Accelerator Ion Sources," IEEE Trans. Nucl. Sci., NS-16, 3, (June 1969).
2. Th. J. M. Sluyters, et al., "A Bright High Gradient 750 keV Ion Gun," BNL Accelerator Dept. Int. Report, AGS Div. 69-11.
3. C. Agritellis, R. Chasman and Th. J. M. Sluyters, "Design of the Low Energy Beam Transport System of the Brookhaven 200-MeV Injector Linac," IEEE Trans. Nucl. Sci., NS-16, 3, (June 1969).
4. J. Aggus and J. Keane, "Linac Tank Installation and Tune-up for the 200-MeV Linac," ibid.
5. R. Damm, V. LoGrasso and A. Otis, "Quadrupole Focusing System for the 200-MeV Linac," ibid.
6. J. Keane, R. Lankshear and A. McNerney, "Summary of the BNL 200-MeV Linac High Power RF System and Its Initial Operating Performance," ibid.
7. S. Dinaro and V. LoGrasso, "Vacuum System for the BNL 200-MeV Linear Accelerator," ibid.
8. N. Fewell and R. L. Witkover, "Automatic Electronic Emittance Device for the BNL 200-MeV Linac," ibid.
9. M. Lee, I. Weitman and R. L. Witkover, "Phase Control and Frequency Control of the 200-MeV Linac for the AGS," ibid.
10. A. Benton, R. Chasman and C. Agritellis, "Computer Calculations of Effect of Space Charge on Longitudinal Beam Dynamics in Proton Linear Accelerators," IEEE Trans. Nucl. Sci., NS-14, 3 (June 1967).
11. R. Chasman, "Outline of a Six-Dimensional Particle Motion Program with Space-Charge Forces for Linacs," BNL Internal Report, AGSCD-31, (Feb. 1968).
12. R. Chasman, "Numerical Calculations of the Effects of Space Charge on Six-Dimensional Beam Dynamics in Proton Linear Accelerators," Proc. 1968 Proton Linear Accelerator Conf., BNL 50120 (C-54), p. 372 (1968).
13. R. Chasman, "Numerical Calculations on Transverse Emittance Growth in Bright Linac Beams," IEEE Trans. Nucl. Sci., NS-16, 3 (June 1969).

TABLE II

CHARACTERISTICS OF THE SOURCE

FILAMENT CURRENT	30A
ANODE VOLTAGE	250V
MAGNET (turns 500)	1.5A
DISCHARGE CURRENT	35A
PULSE LENGTH	120 μsec
PRESSURE	$\approx$1 mm
BEAM CURRENT	370A
PROTRON PERCENTAGE	>80%
NORMALIZED PHASE SPACE AREA ($\beta\gamma$A)	1.4cm-mrad

GEOMETRY OF THE EXPANSION CUP

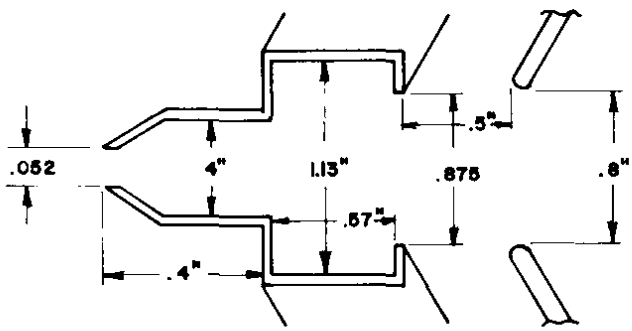

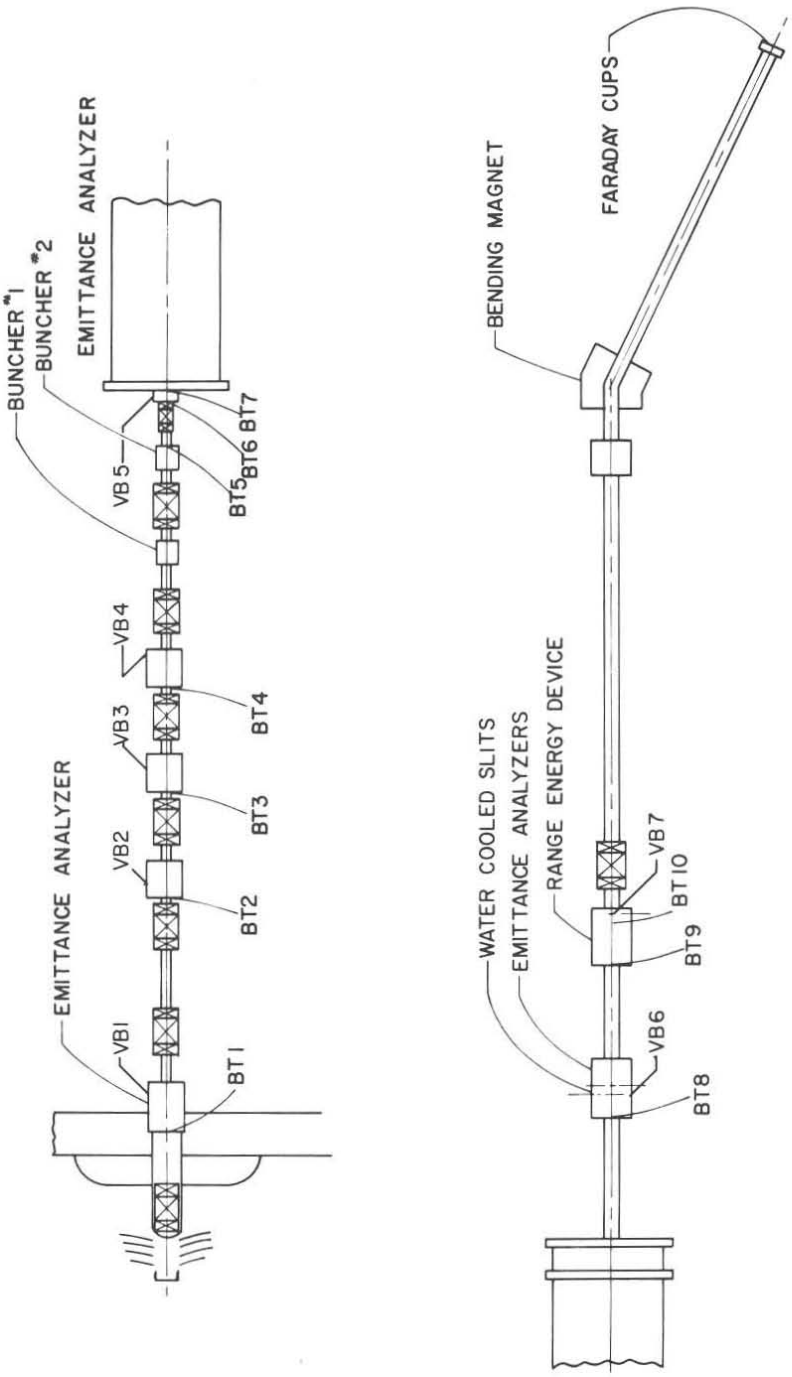

EQUIPMENT LAYOUT
Fig. 1

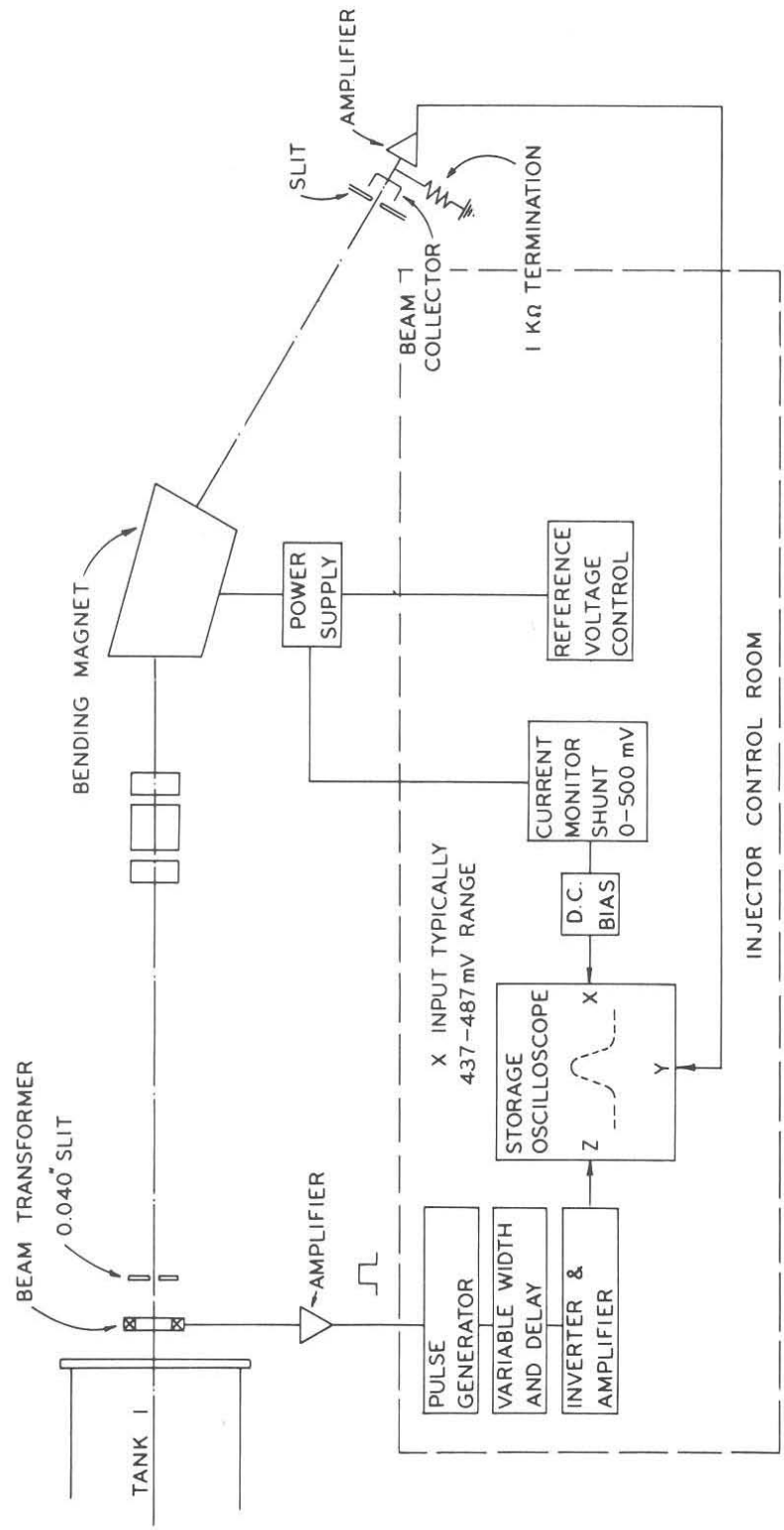

EQUIPMENT USED FOR MOMENTUM MEASUREMENT

FIG. 2

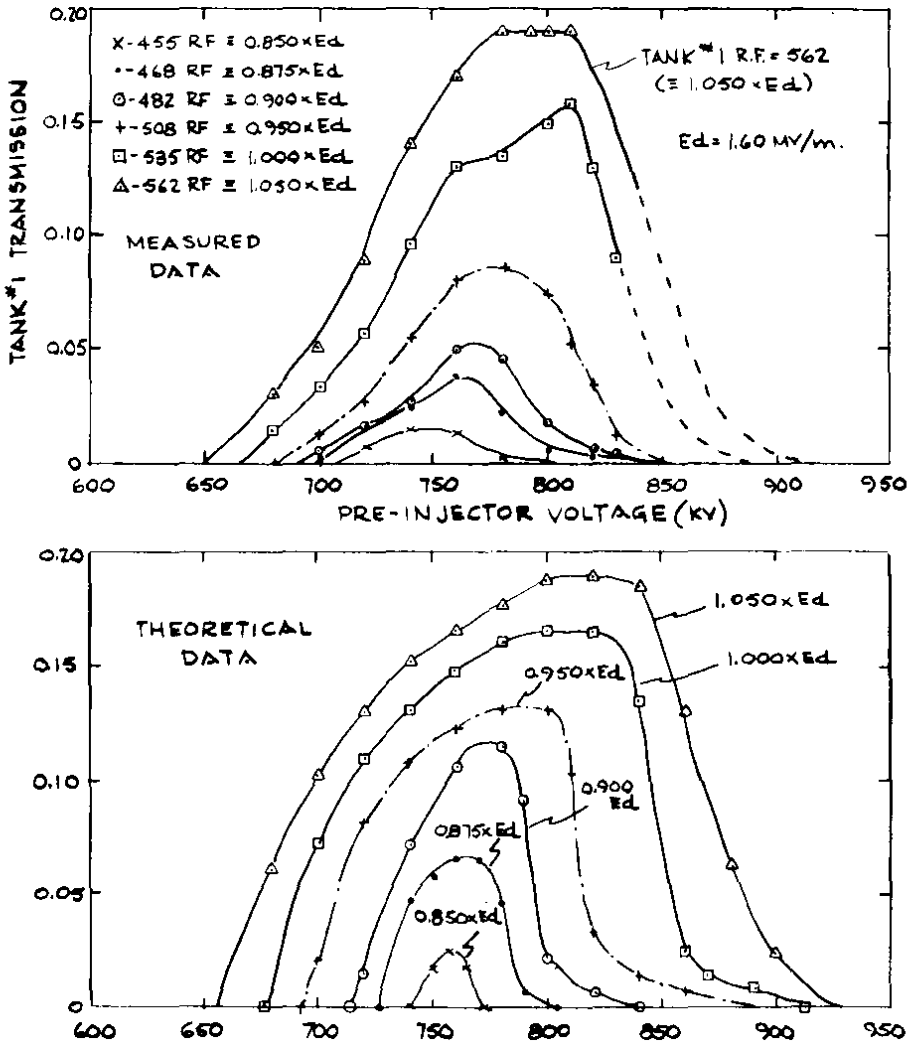

10 MeV BEAM CURRENT AS A FUNCTION OF PRE-INJECTION ENERGY (NO BUNCHERS)

Fig. 3

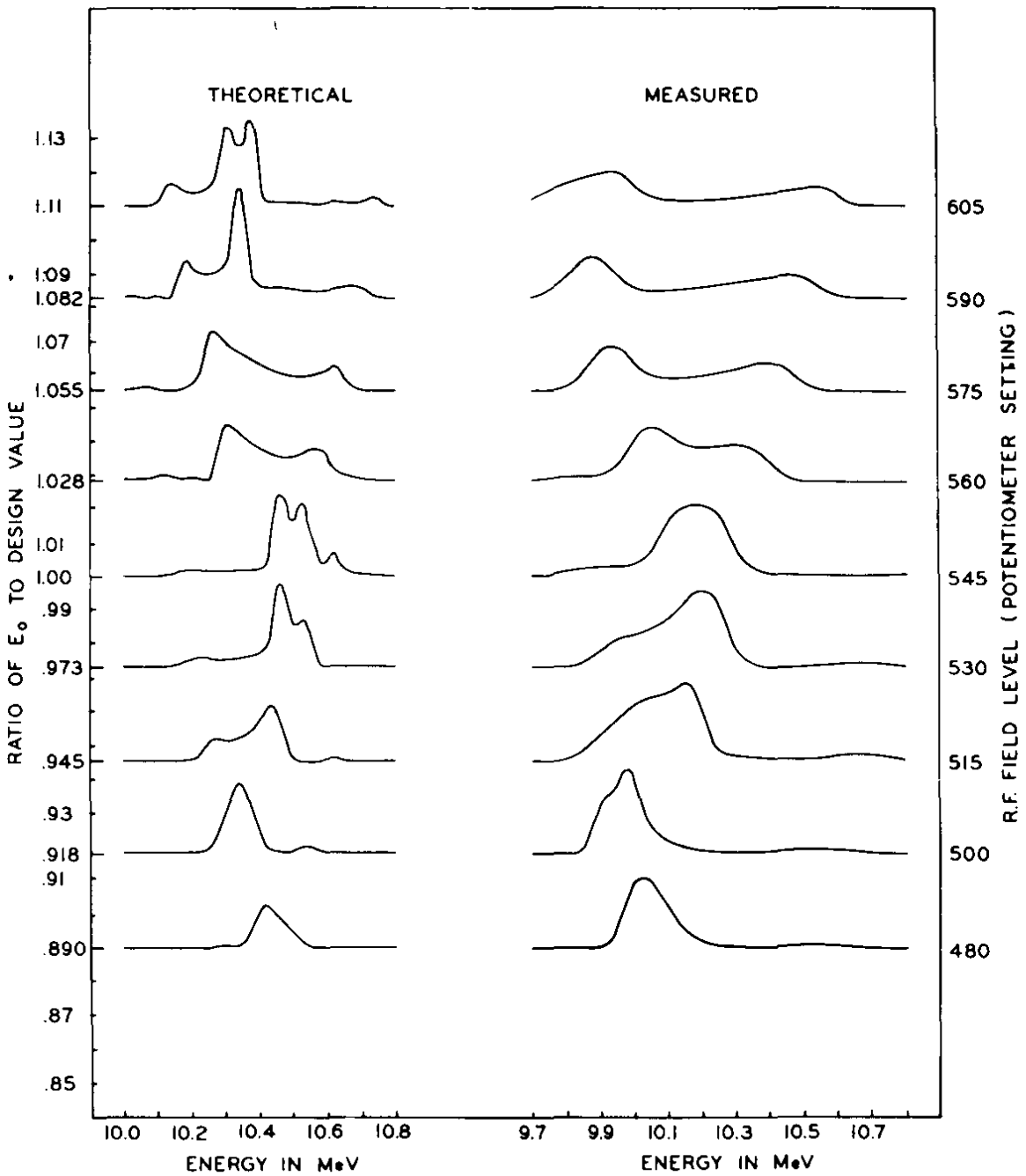

ENERGY SPECTRA AS A FUNCTION OF TANK I R.F. LEVEL
FOR 730 KeV INJECTION ENERGY (NO BUNCHERS)

FIG. 4

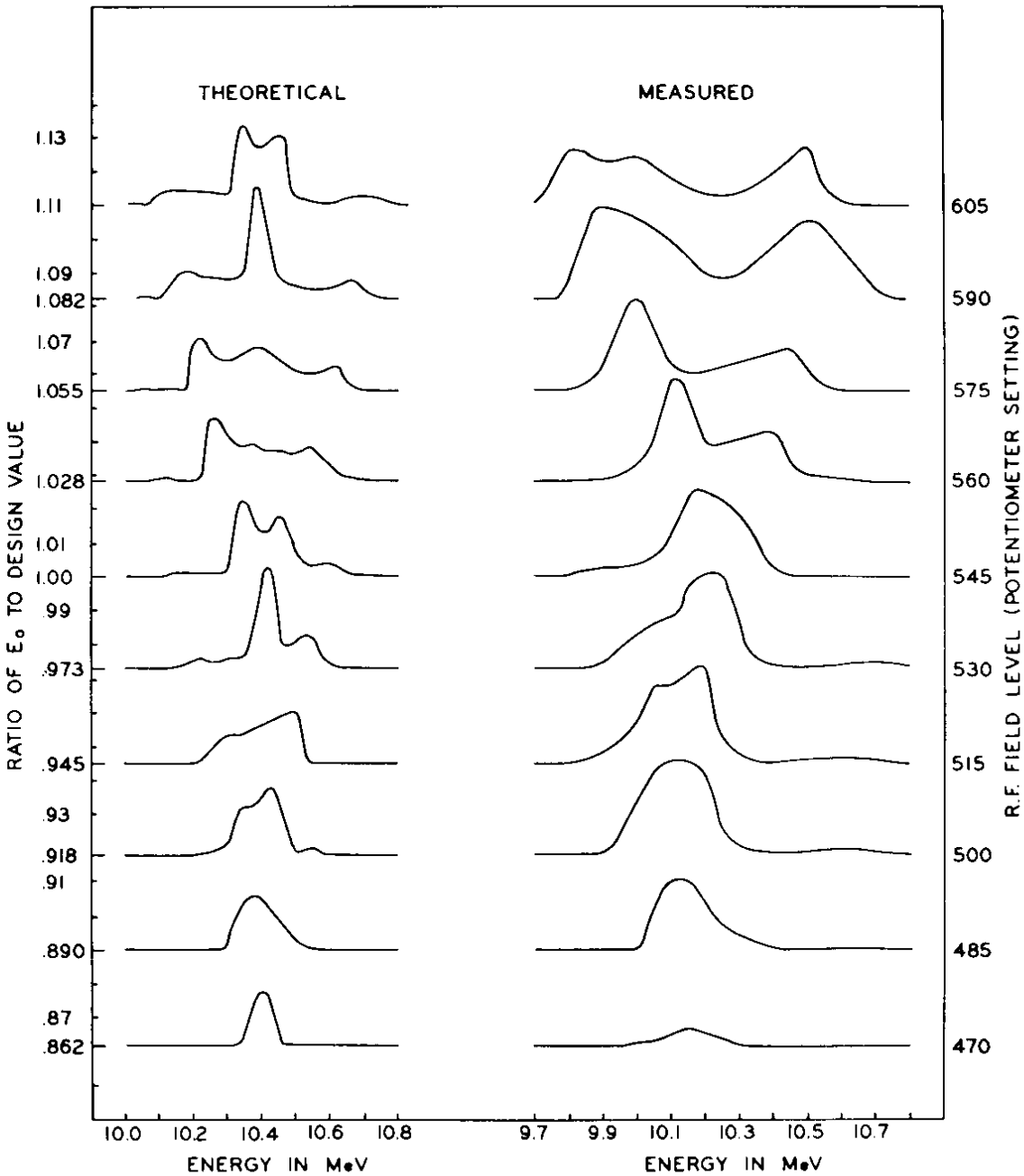

ENERGY SPECTRA AS A FUNCTION OF TANK I R.F. LEVEL
FOR 750 KeV INJECTION ENERGY (NO BUNCHERS)

FIG. 5

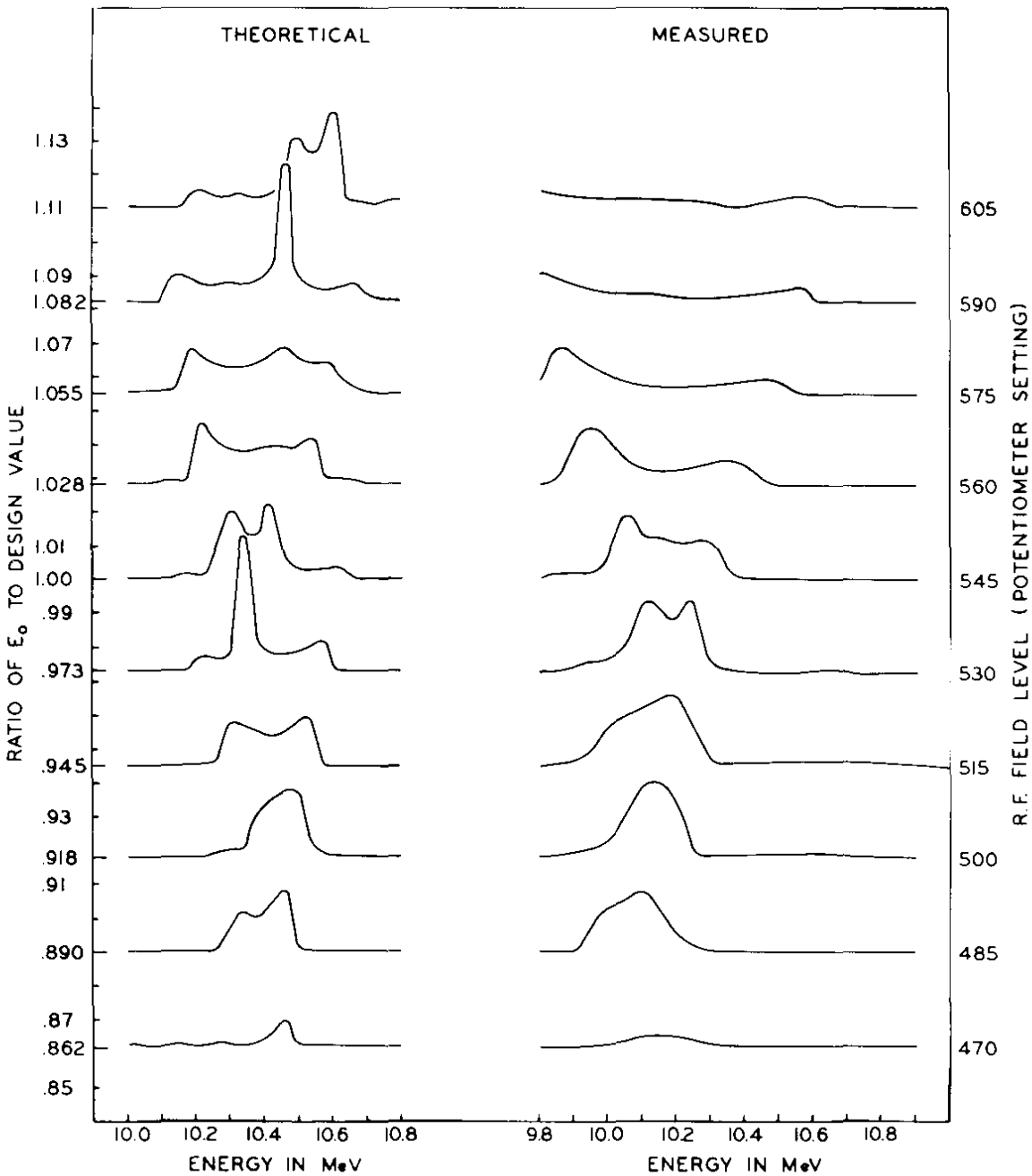

ENERGY SPECTRA AS A FUNCTION OF TANK I R.F. LEVEL
FOR 770 KeV INJECTION ENERGY
(NO BUNCHERS)

FIG. 6

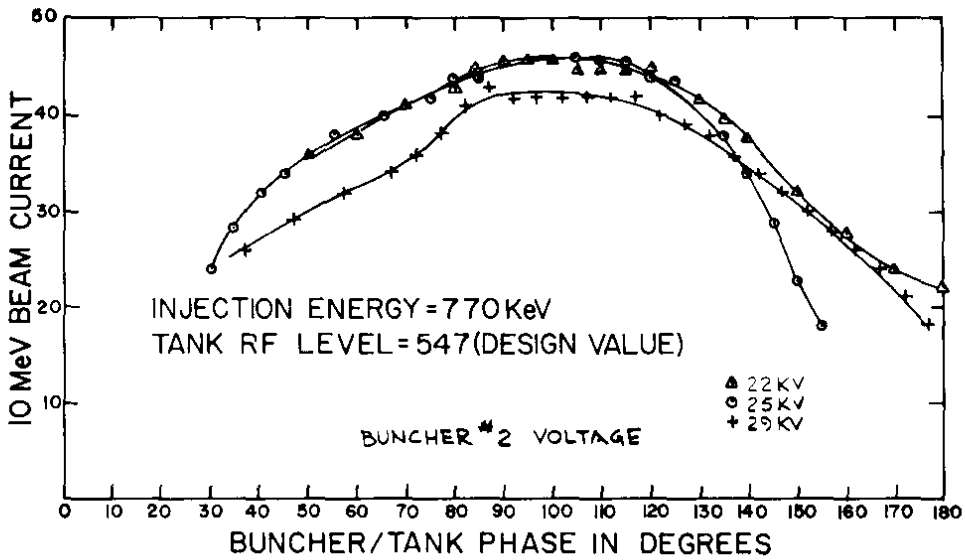

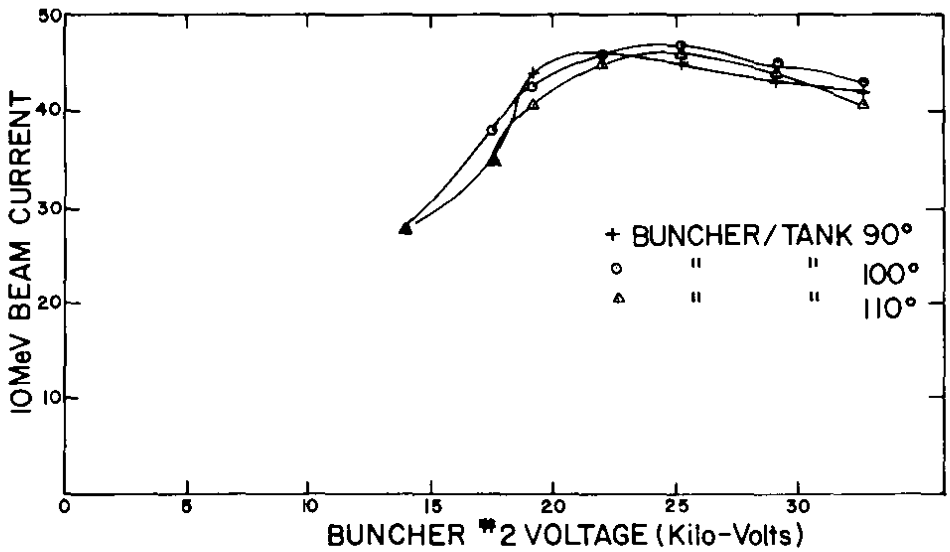

OPTIMISATION OF BUNCHER #2

Fig. 7

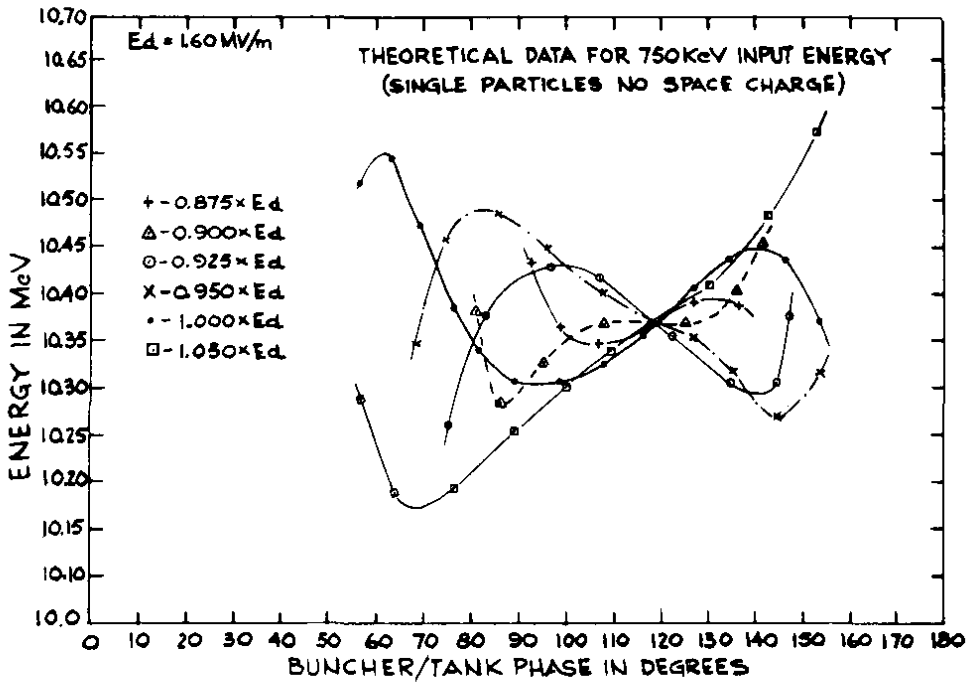

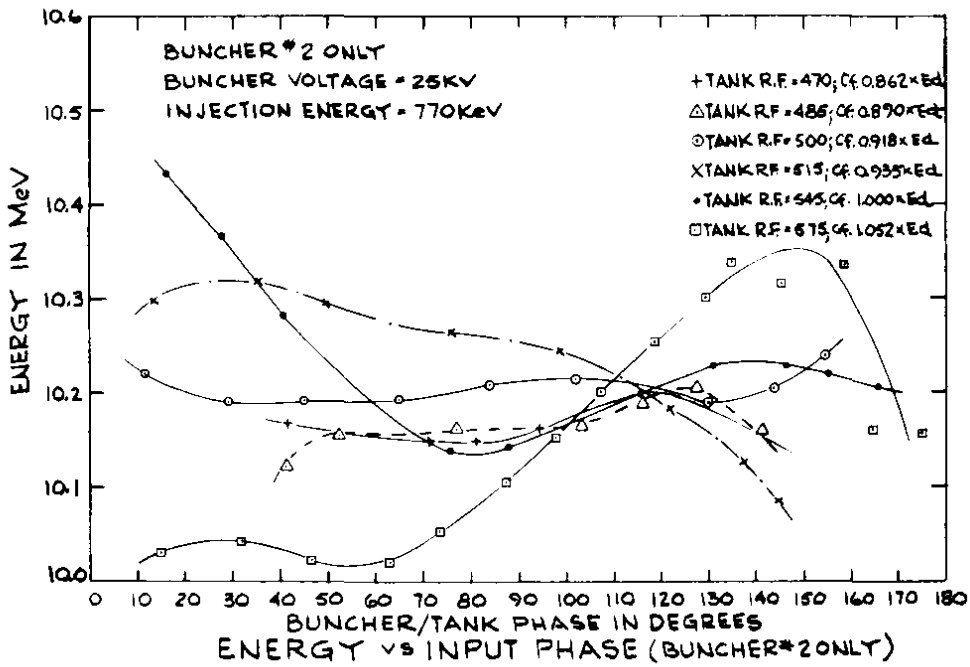

ENERGY VS INPUT PHASE (BUNCHER #2 ONLY)

Fig. 8

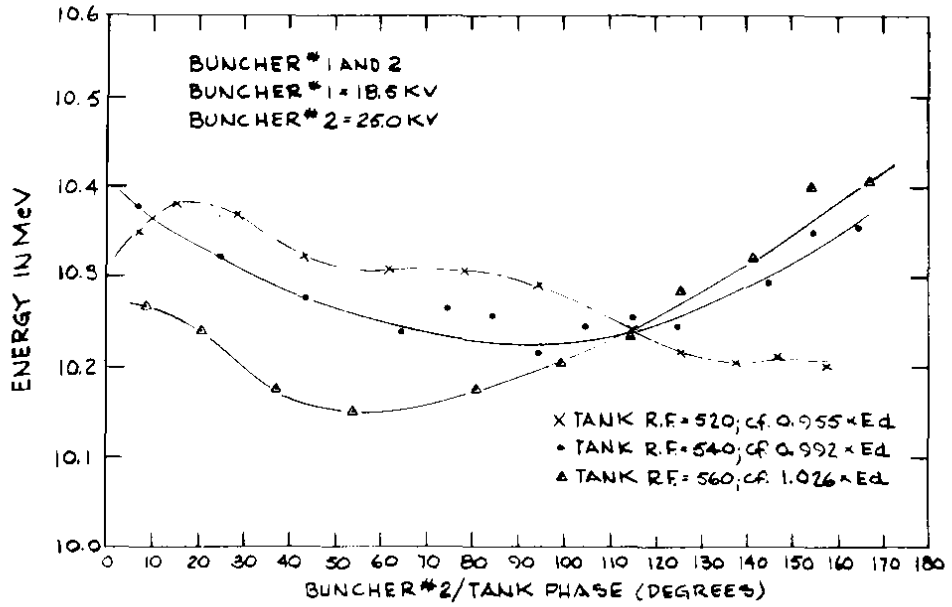

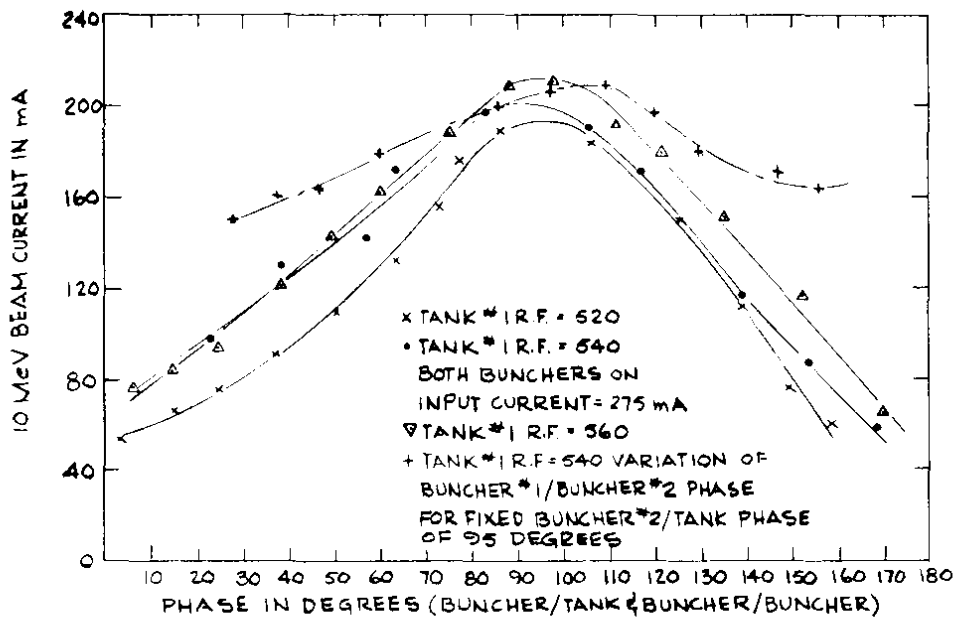

ENERGY & BEAM CURRENT VS INPUT PHASE
(BOTH BUNCHERS)

Fig. 9

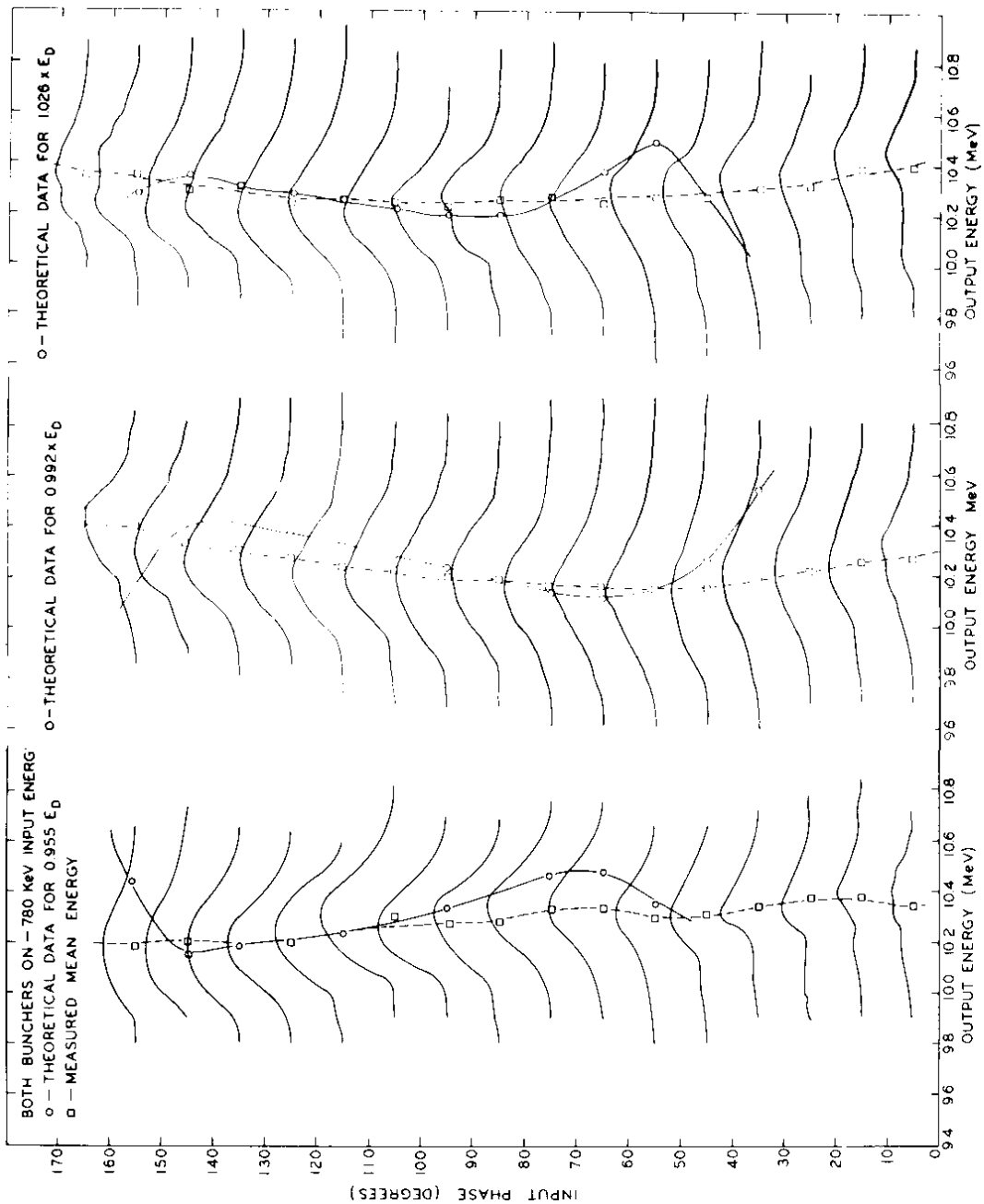

ENERGY SPECTRA VS INPUT PHASE FOR 210 mA OUTPUT BEAM CURRENT

FIG.10

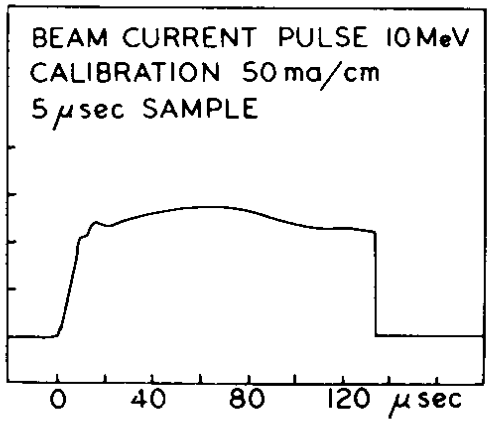

BUNCHER 1 = 16.8 KV BUNCHER 2 = 24.4 KV
TANK 1 R.F. LEVEL = 540 (DESIGN VALUE)
PREINJECTOR = 780 KV

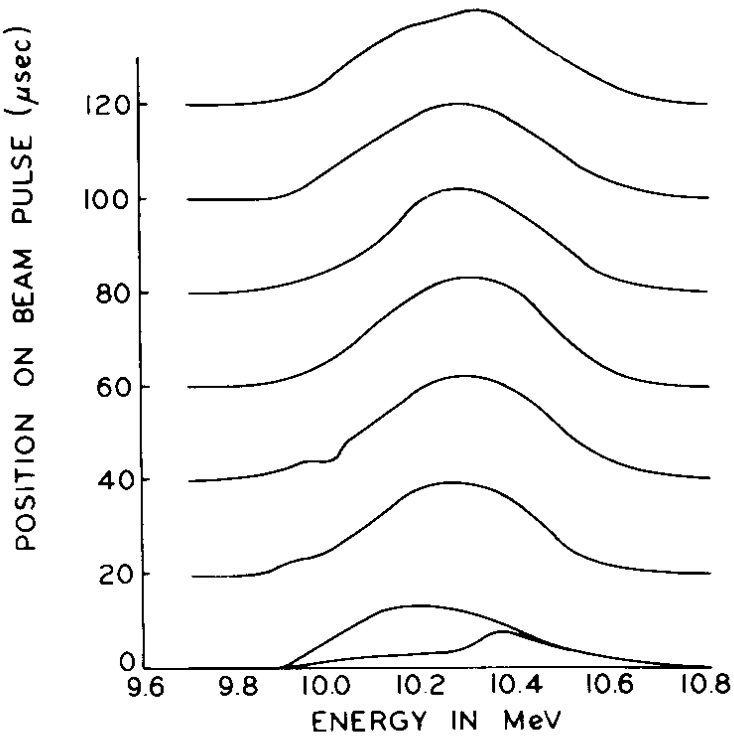

10 MeV SPECTRA AT VARIOUS TIMES DURING THE BEAM PULSE

FIG. 11

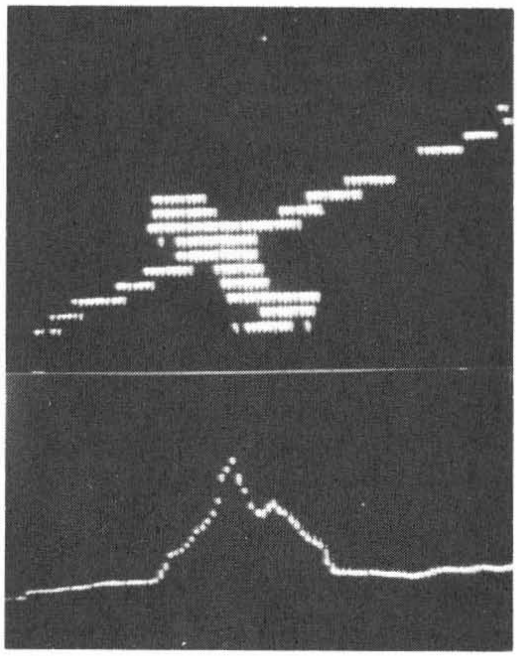

AN EMITTANCE AND DENSITY DISTRIBUTION FOR A 300 mA BEAM MEASURED DIRECTLY AFTER THE PREINJECTOR AT 760 keV. TOTAL EMITTANCE AREA IS 34 cm-mrad (NORMALIZED 1.36) FOR 90% OF THE BEAM.

Fig. 12

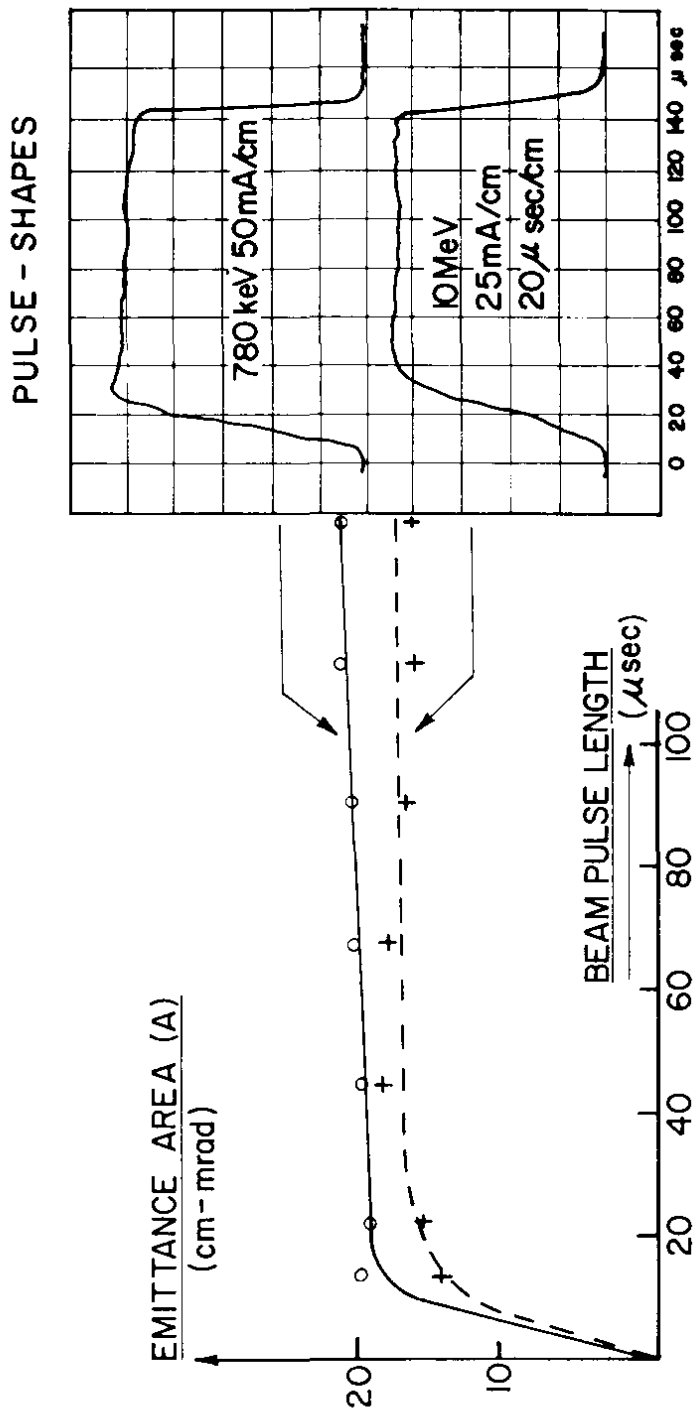

Fig. 13 EMITTANCE AREA AS A FUNCTION OF POSITION DURING PULSE

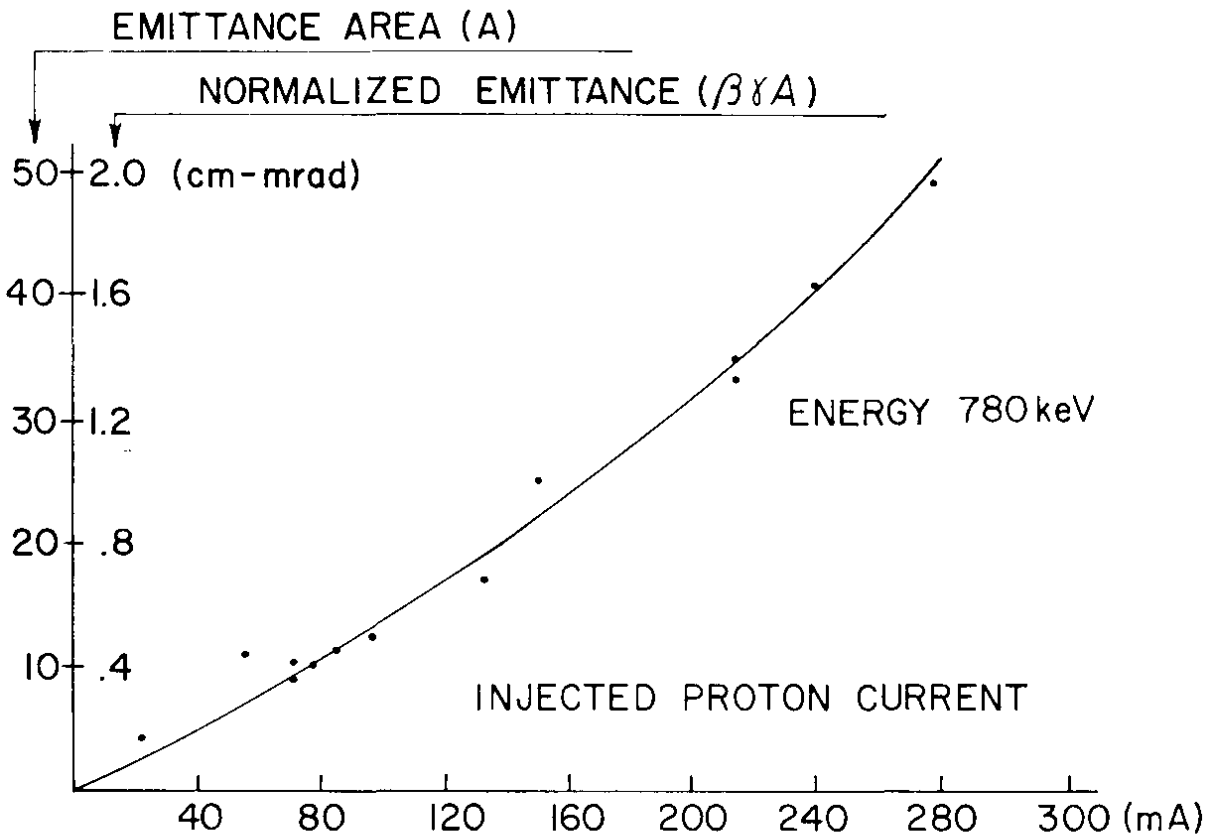

Fig.14 EMITTANCES FOR OPTIMIZED BEAM CURRENTS

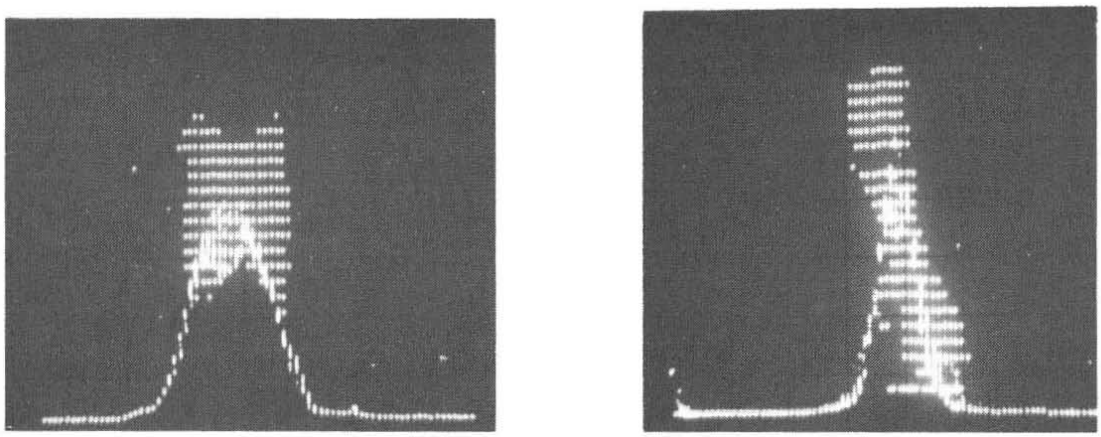

Y-Y' X-X'

TYPICAL EMITTANCE IN THE X-X' AND Y-Y' PHASE PLANES FOR NEARLY IDEAL MATCHED BEAMS. THIS EXAMPLE IS A 240 mA INJECTED PROTON BEAM RESULTING IN A 140mA LINAC OUTPUT.

Fig.15

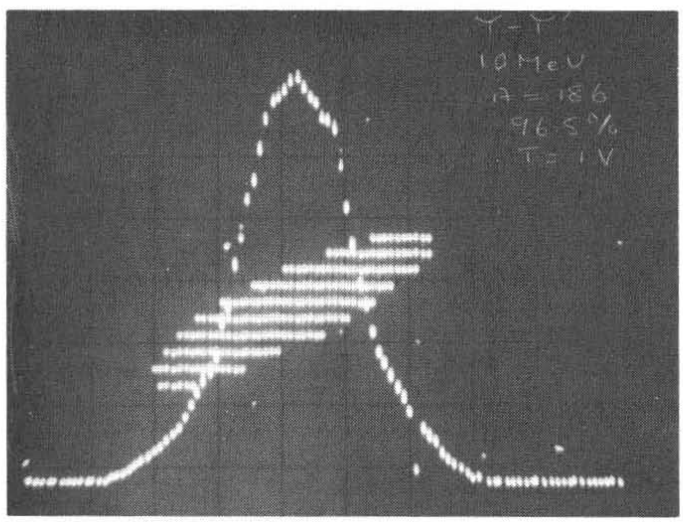

TYPICAL EMITTANCE PATTERN FOR BOTH PHASE PLANES AFTER ACCELERATION AT 10MeV (140mA).

Fig. 16

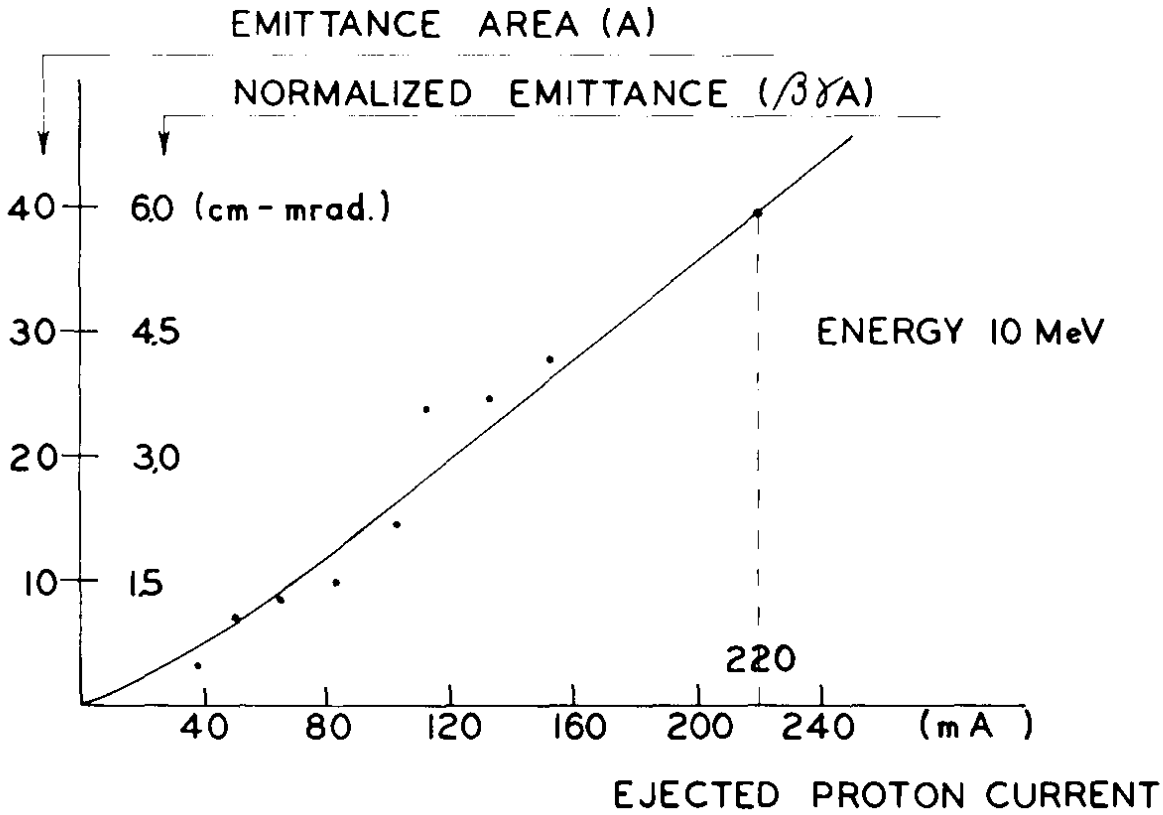

Fig.17 EMITTANCES VERSUS OUTPUT CURRENT

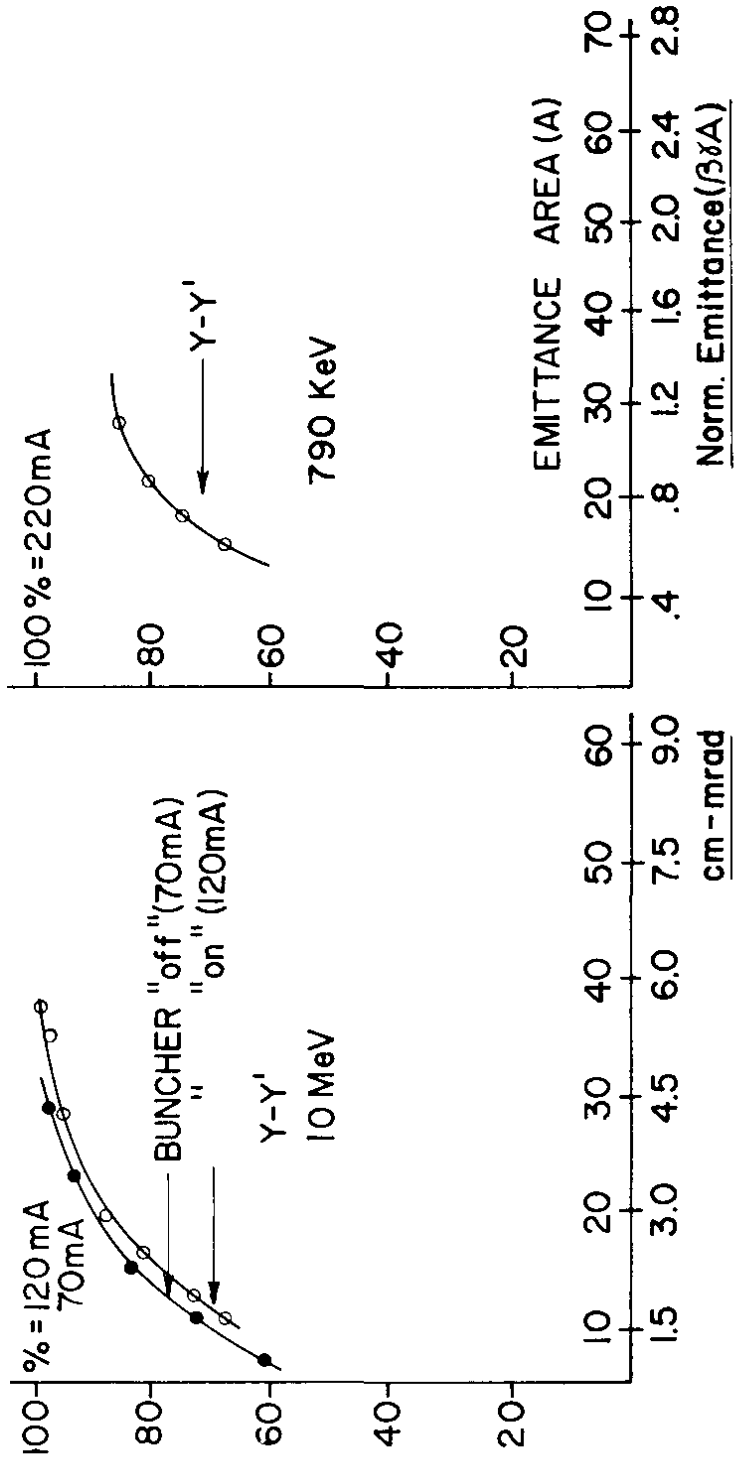

Fig.18 TRANSVERSE LINAC PERFORMANCE IN THE Y-Y' PHASE PLANE AND 55% TRANSPARENCY.

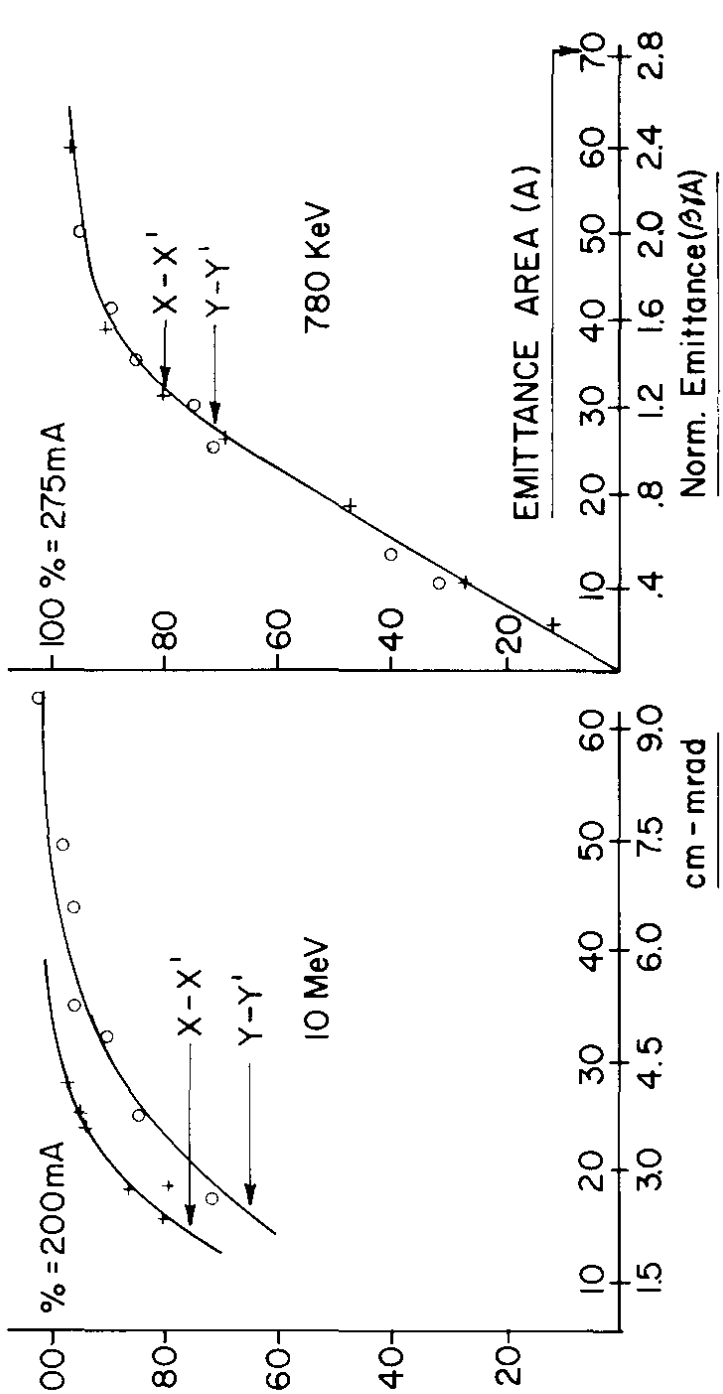

Fig.19 TRANSVERSE LINAC PERFORMANCE WITH 72% TRAPPING EFFICIENCY

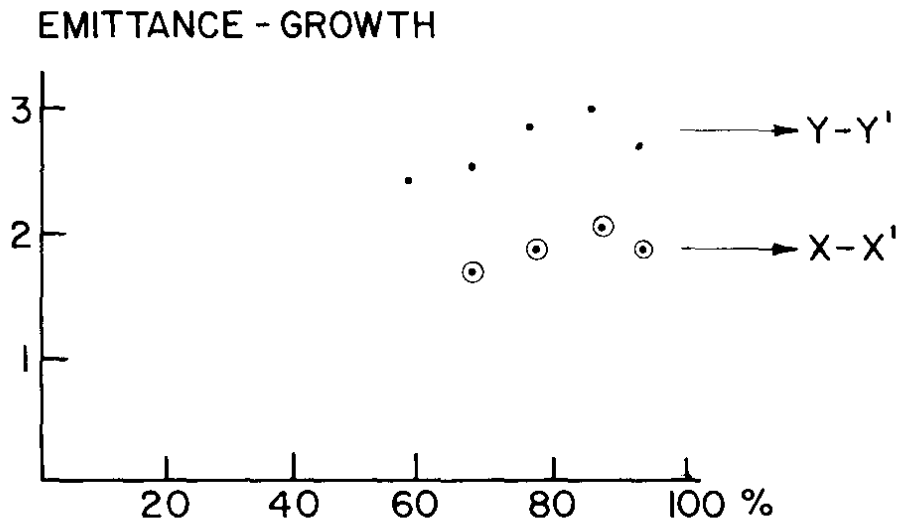

Fig. 20 EMITTANCE GROWTH IN THE FIRST TANK FOR A 200 mA BEAM.

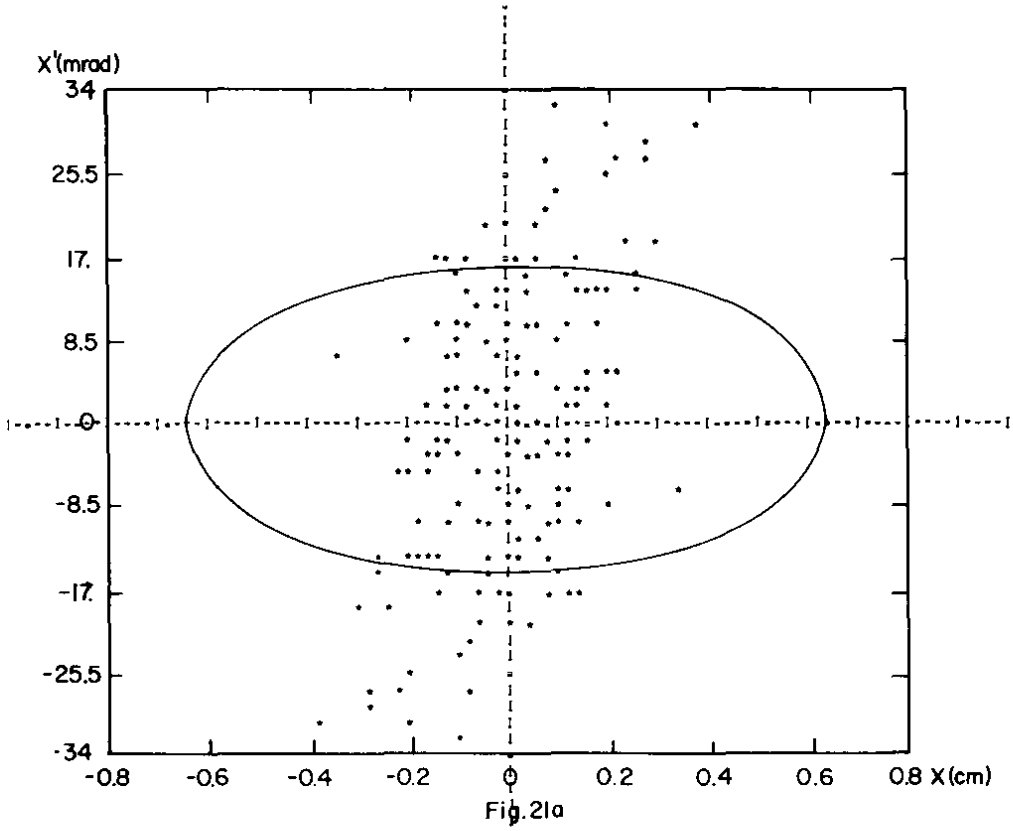

Fig. 21a

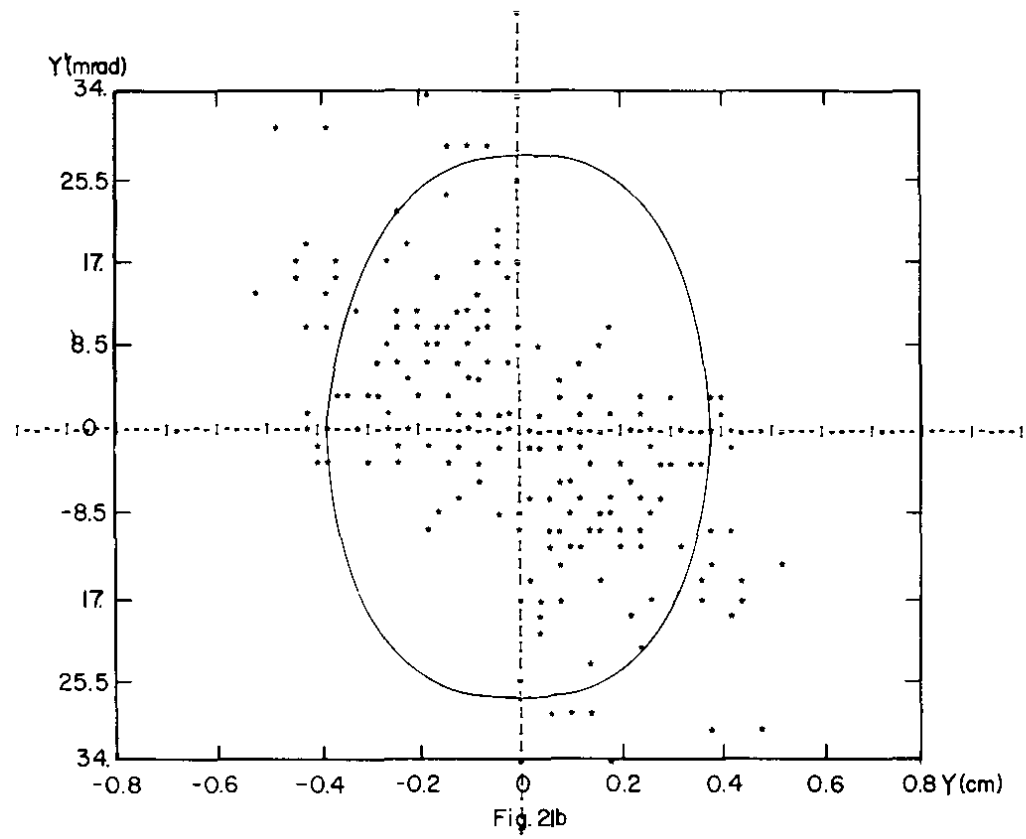

Fig. 21b

Fig. 21 Calculated emittances at center of drift tube 3 in linac.

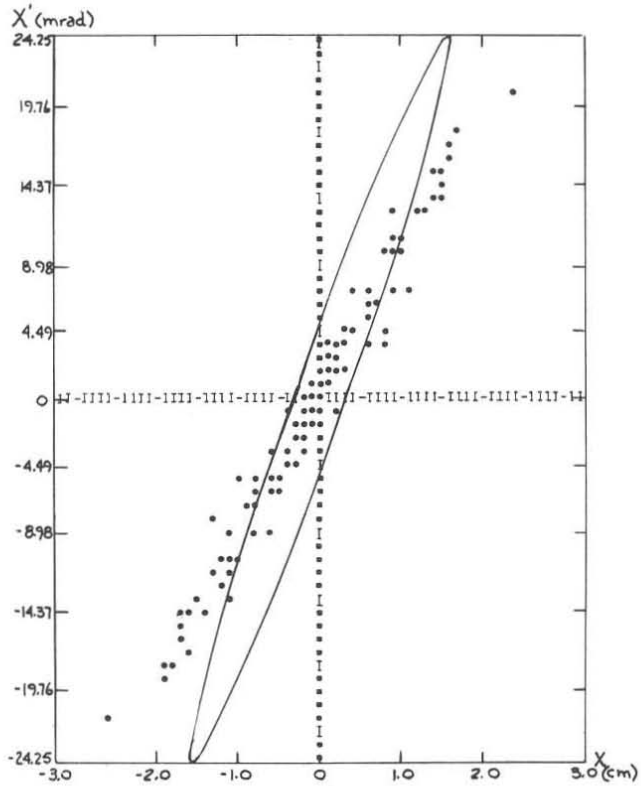

Fig. 22a

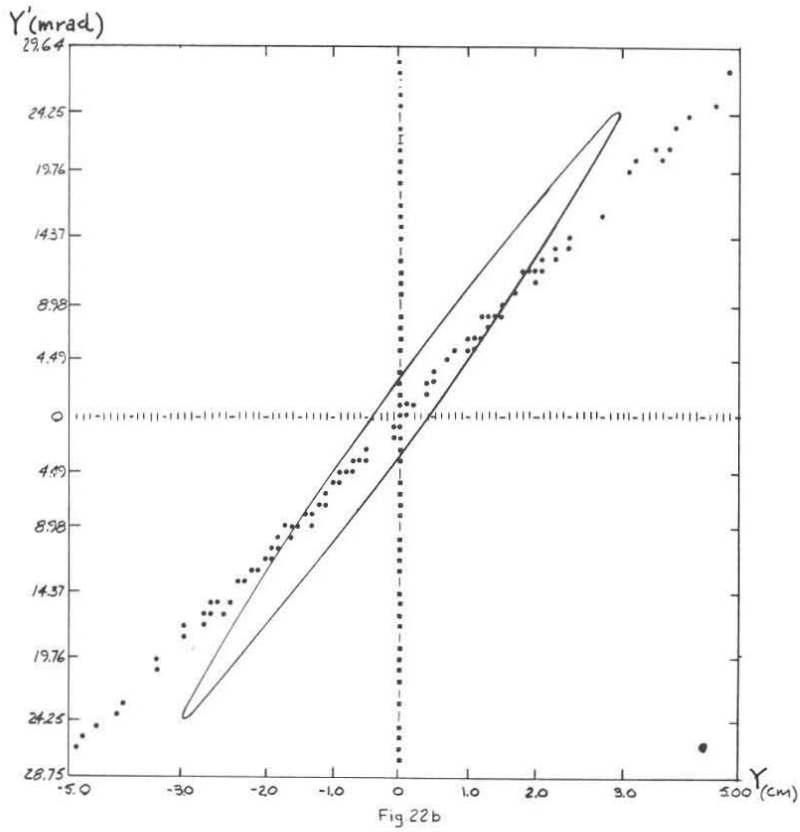

Fig. 22b

Fig. 22. Calculated emittances at VB #6.

DISCUSSION

C. D. Curtis (NAL): Could you give a number for the energy spread?

K. Batchelor (BNL): At 200 mA, there is 500 keV full-width, half-height energy spread. This spread is essentially independent of beam current.

C. D. Curtis: We found the same behavior as a function of beam current.

E. Regenstreif (Rennes): Why is the emittance growth larger in y than in x?

K. Batchelor: That is not clear. We were never matching properly from the pre-injector, which is probably one of the causes. But the matching in x was worse than that in y.